Single-material coupling-tolerant semi-planar microresonator using Littrow diffraction

Henri Benisty

Single-material coupling-tolerant semi-planar microresonator using Littrow diffraction

Henri Benisty

Laboratoire Charles Fabry de l'Institut d'Optique, CNRS, Univ. Paris-Sud, Campus Polytechnique, RD 128, 91127 Palaiseau Cedex, France

Resonators carved in a single material such as disc, rings, spheres, do not require genuine mirrors since they exploit shape resonances, but they then suffer from poor coupling to standard free-space collimated beams. Exploiting the idea of Littrow resonators combining total internal reflection and grating diffraction, we propose trapezoidal prism-type geometries that include a strong grating on one face, and total internal reflection on the other face. Resonant modes are localized within a length of the same order as the prism thickness, but are well coupled to free-space beams. The resonator core can be seen as a broad waveguide with multimode coupling of ''Littrow modes'', a configuration recently pointed out for its capability to produce a ''collective'' slow-light regime. A more ''planar'' version, with a saw-tooth input-coupling grating for vertically collimated beam is also proposed.

Keywords: Resonators; Gratings; Littrow diffraction; Surface coupling; Flat bands; Slow light

1. Introduction

Micro- and nano-resonators are currently elaborated along a number of selected technological options. Rings, toroids, discs, spheres exploit simple shapes involving near-total internal reflections to attain very high quality factors Q [1]. Due to the symmetry of the resonant mode, engineered coupling to the outside is practiced either with a tapered fiber section or a coupling waveguide with a mastered air gap (Fig. 1(a) and (b)). Coupling directly to a free-space collimated beam is notoriously delicate in such systems, triggering attempts such as the modified spiral disks, Fig. 1(c) [2,3]. The resulting systems offer still a coupling much poorer than that of a more traditional Fabry-Perot etalon (Fig. 1(d)). The miniaturization of a Fabry-Perot to a small size is a very well documented topic in optoelectronics since the advent of VCSELs (vertical cavity surface emitting lasers), two decades ago, and correlatively, the publication of numerous studies on micropillars in relation with quantum electrodynamics (QED) effects in the solid-state [4]. However, such structures involve layered stacks as a starting point, and preferably, with a high index contrast. Hence, the fabrication has to cope with, e.g. the differential etching behaviour of these layers (AlAs and GaAs in model systems), so that demands on shape optimization (see e.g. [5,6]) find certain limits, in theory as well as in practice [7]. Also, intrinsically, a multilayer system is prone to delaminating when submitted to a high peak power, whereas a fundamentally single-material structure is more resilient to optical damage, with a fluence-limited

E-mail address: henri.benisty@institutoptique.fr.

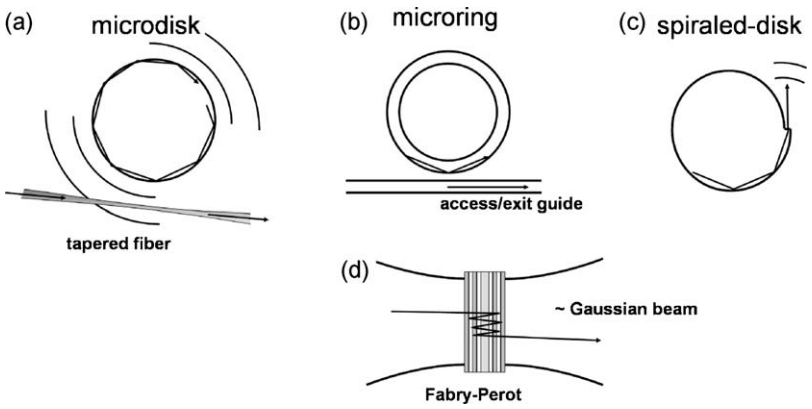

Fig. 1. Confinement schemes using a single piece of material: (a) microdisk; (b) microring addressed by a ''bus'' waveguide; (c) spiraled disk; (d) Fabry-Perot with multilayer mirrors, common in VCSEL devices, or microcavity LEDs.

by the material's properties (silica for example, in toroids), both in the bulk and at its surfaces. Spectrally, the use of several materials is also a constraint. The spectral range narrows down because it is the intersection of the several constituent materials' ranges. This often prevents exploitation of nonlinear phenomena. For linear use, for example, Born and Wolf's optics textbook [8] evokes the (obsolete) Gehrcke-Lummer interferometer, a single slab of quartz used at grazing angle, that was unique for providing the high Fabry-Perot-type resolving power in ultraviolet, the best solution during several decades. Other single-material resonators include triangular ones or square ones [9–14], with, likely, similar considerable coupling difficulties to standard beams, although nice directionality effects *in emission* are seen in targeted geometries. Integrated optics offers an alternative path, coupling from, e.g. a fiber to a waveguide and implementing the resonant elements aside the waveguide. This approach has its own merits but suffers from severe limits when it comes to consider both criteria of low losses and miniaturization. Interesting miniaturization of a fiber coupler to SoI (silicon-on-insulator) waveguide [15] not only showed some promises but also highlighted difficulties of this approach.

In this context, we tackle the following issue: can other shapes be devised, retaining the essence of the single-piece and single-material aspect (forbidding gaps between parts and allowing at most one supporting planar interface such as silica/silicon)? Still we want to retain direct coupling to a collimated, or weakly convergent free-space beam, e.g. like those of usual fibers (roughly a 3–8 μm spot for a 1.5 μm wavelength).

The motivation for this quest, beyond curiosity, is to find geometry for enhanced light-matter interaction, that lend themselves to implementation in highly parallel and robust optical systems. In optoelectronics, the cost of edge emitting laser diodes is hampered by the need to cleave before test, an inconvenience circumvented by VCSELs, that lend themselves optimally to quick and extensive on-wafer testing. In the same spirit, we foresee that a wafer surface could be packed with our proposed device. Application for cheap photopumped lasers can be envisioned, with many multiple colors side by side, for miniature agile sources in the visible for example. Another possibility is to consider sensors and in particular biosensors. A highly resonant mode transforms a small amount of hybridized biochemical material, spatially immobilized in its optical mode, into a larger signal than a non-resonant one. This signal can be a change in reflection/transmission, or a fluorescent signal. In the area of arrayed biochips, the ''spots'' could be brought onto the corrugated surface of our resonators. Parallelism then not only serves both the biological needs (say, many proteins have to be screened) but also the need for acceptable calibration through redundant control devices. With micro-optics probe adapted to the beams that we in-couple or out-couple in this study, the volume of the optical part of the sensor could be shrunk to the cm^3 range, while still benefiting from either the advantages of fluorescence (high sensitivity and selectivity) for labeled molecules or from increased sensitivity for non-labeled probing, e.g. through modulation of the index of refraction at the surface.

Our positive answer to the issue of the single-material single-piece resonator, relies on the properties of broad waveguides that incorporate deep gratings on one of their surface. The generic effect of a grating of period Λ is to resonantly couple those modes of the waveguide that differ by the lattice reciprocal wave-vector, $K = 2\pi/\Lambda$. A particular case in such broad guides concerns ''oblique'' modes, i.e. modes whose constituent plane-waves are more oblique than those of the

fundamental mode, but still below the relevant light line of the system ($k_{//} > n_{\mathrm{clad}}\omega/c$, with $k_{//}$ the wavevector along the guide and n_{clad} the cladding index). For the proper period/frequency/angle combination, such waves are retro-reflected, a case known as the Littrow mount, popular in external cavity lasers. We recently found [16] that in the dispersion region associated with this Littrow diffraction, a bunch of waveguide modes can be shaped into very flat bands for a critical coupling value, that is for a critical (and large) diffraction efficiency. Based on this property of an infinite system – ''collective'' flat bands – a finite system, when properly bounded, is shown to result in a high finesse resonator. The flat bands mean that light does not easily propagate. It prolongs its local lifetime, being forced to undergo several local round-trips before it can actually propagate. At the very band edge, in a 1D periodic system, any of the modes is a pure standing wave with zero group velocity. If proper boundary conditions are provided, this long photon lifetime is also reflected in a high quality factor and a high finesse of the resulting resonator.

We discuss in this paper the application of this strategy to a broad waveguide lying onto a silica substrate. The guiding material index has to be high enough (e.g. $n \sim 3$ or above, as in Si) to provide internal reflection at around 45°, and also to ensure the virtual suppression of light leakage upon *internal* Littrow back diffraction at the grating. A trapezoidal prism-based geometry, which can be intuited from ray-tracing, is first analyzed. The typical period Λ is $\sqrt{2}$ larger than in standard feedback devices, due to the smaller $k_{//}$ value along the grating, hence around 300 nm for $n \sim 3$ and 1.5 μm range, or around 200 nm if one approaches the near infrared regime ($\lambda \sim 1$ μm). At this point, it is worth noting that lower indices are in principle possible, provided total internal reflection is ensured with more glancing angles of incidence (50–70°). But several drawbacks creep in for such conditions. We only list them briefly here: (i) the substrate index should provide sufficient margin, it is hard to think of anything realistic lower than $n = 1.4n$ demanding therefore prism indices above $n \sim 1.8$. (ii) At the most glancing angles, the interaction with the grating on top diminishes, increasing the difficulty to get internal ''blazed'' Littrow reflection and high-Q. (iii) The in- and out-coupling also become more difficult and less tolerant since, in essence, this situation tends toward traditional guided wave devices with usual facets.

To start our study, the resonant modes are first evidenced in transmission mode. Their rather large angular tolerance is then made clear. Designing an optical microcavity with a view to its instrumental properties (pupil, aperture, field acceptance) has been scarcely addressed as a ''nanophotonic'' issue until now, while it may prove crucial for a widespread use of such systems. The photonic crystal (PhC) community has recently tackled its own version of this issue in order to get acceptable beams from the very-high-Q nanocavities with sixfold symmetry ([17]) whose ''beaming'' is more easily obtained than the very successful cavity family stemming from S. Noda seminal work in 2003 and 2005 [18,19] (Lee's team also examined the coupling of modified PhC cavities to tapered fiber [20]). But the PhC resonator strategy, in spite of the huge inspiration it has triggered in the past decade, is limiting the options when it comes to thinking about such resonator as a ''standard'' micro-optical component, which has to be inserted on a miniature bench among many others, not precluding future progresses though.

After the trapezoidal prism-type geometry study, which may be coined as a ''semi-planar'' approach, we seek a more planar resonator, offering notably a near-vertical free-space beam coupling on a wafer. For this, we replace the entrance and exit facets of the prism by two double-period saw-tooth gratings. The study is currently limited to one polarization and to two dimensions, but this is enough to provide the most delicate design rules to be obeyed for such microcavity components. Section 2 gives a more precise picture of the modes in the cavity. Section 3 analyses the trapezoidal prism-type system. Section 4 deals with the top-access one. Section 5 is the conclusion

2. Modal analysis of "Littrow modes"

2.1. Model of coupled waveguide modes, critical coupling

To build up the microcavity, we analyze in this section how light is slowed down (bands are flattened) in a thick corrugated waveguide, much as the large photonic crystal waveguides were we first observed ''Littrow lasing'' [21].

The analysis, partly presented in [16], relies on the basic modal decomposition of a general Bloch mode on the ordinary propagative waveguide modes (Fig. 2(a)) unaffected by the corrugation. These latter, for a width W (which may be later an effective width) take the form

$$E \sim E_0 \sin(k_x x) \exp(jk_z z - j\omega t) \tag{1}$$

with confinement inducing a quantized transverse momentum $k_x \approx \pm m\pi/W$ ($m = 1, \ldots, m_{\max}$).

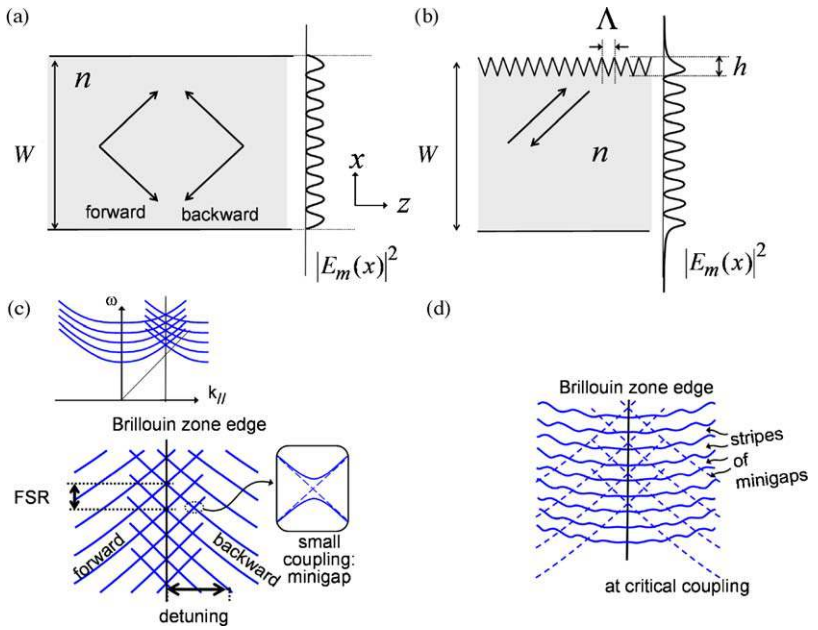

Fig. 2. Physics of multimode broad corrugated waveguides: (a) basic modes in non-corrugated waveguides; (b) build of Littrow diffraction among modes due to the corrugation; (c) band structure with Brillouin zone edge folding and expected coupling loci (enlarged below); (d) schematic appearance of stripes of minigaps upon strong enough coupling.

This form entails a dispersion relation of the form

$$\omega = \frac{k_z c}{n_{\text{eff}}(k_z)} = \frac{c}{n}\left(k_x^2 + k_z^2\right)^{1/2} \tag{2}$$

The presence of the grating cannot, rigorously, be treated as a perturbation, because for thick gratings, the mode profile is repelled inside the material in a specific fashion, but this does not matter at the present stage. Rather, some essential features can still be obtained in this frame.

As the grating is formed, minigaps form at the intersection of the dispersion branches $m = 1, \ldots, m_{\max}$ with their folded counterparts (Fig. 2(c) and (d)), due to a mode coupling taking place between all guided modes of Eq. (1), save for selection rules induced by possible guide symmetries. For a grating of some strength, these minigaps tend to merge, and form "stripes of minigaps" [22] repelling bands. Furthermore, when the coupling strength is increased to a critical value (Fig. 2(d)), bands located between the stripes of minigaps become themselves optimally flat, forming a series of branches that mimic, in shape, those of a Fabry-Perot resonator, albeit with dispersion minima offset at the zone edge.

At this stage, we are in the presence of a particular form of multimode slow light, with branches regaining wiggles of some amplitude when leaving the Brillouin zone edge. But the upper bound to their local group velocity remains much smaller than c/n across many modes and many wiggles. Since the interactions leading to this situation arise among modes essentially described by Eq. (1) above, these interactions can be understood based on a quasi plane wave picture. Coupling is a diffraction event on the grating for these local plane waves, and we may have the situation of a strong local diffraction efficiency of the grating holding over large angular spans and spectral spans. Notably, the angular span may be much larger than the angular separations among successive modes and the spectral span may be larger than the free-spectral range. This situation amounts to attain a high coupling of forward to backward modes, which remains about constant in a wide region of the dispersion diagram $\Delta k\, \Delta\omega$. By comparison, the Fabry-Perot case may be used: the formal group velocity of Fabry-Perot modes is also small, the dispersion is quadratic $\omega^2 = \omega_0^2 + k_{//}^2 (c/n)^2$ leading to $v_g \propto k_{//}$. Our former studies indicate that our situation may lead to slow-down regions whose area in the dispersion diagram, $S_{\text{disp}} = \Delta k\, \Delta\omega$, is comparable to what can be obtained from a Fabry-Perot geometry with standard multilayer mirrors (DBR mirrors for example, as in VCSELs). Of course, the number of modes m that are coupled follows the same trends as modes in a Fabry-Perot, scaling merely with thickness and frequency. For microresonators whose modes are separated by more than 5 nm typically, the thickness is less

than 10–100 μm depending on specific indices and wavelength.

At this stage, we may thus consider a corrugated waveguide as an open resonator. We do not look at the fundamental mode, because it interacts too weakly with the guide boundaries (it yields for example well-separated "mini-stopbands" [23–25] when coupling to higher order modes). Nor do we look at Fabry-Perot modes in the presence of the grating, because the specular reflection may be substantially spoiled by the corrugated nature of the guide boundary. Rather, we look at an open resonator whose underlying plane waves are coupled by Littrow or near-Littrow diffraction. We initially reported on lasing in such structures [21], but without special care for the degree of slow-down, nor for the further localization of the mode in the free (opened) dimension, as it was dependent on the extent of pumping. The work in [16] has given some clues on the degree of slow-down, while in [22], it was possible to highlight the extent of the useful area in the dispersion diagram, $S_{\text{disp}} = \Delta k\, \Delta\omega$, showing that strong photonic DOS modulations, with almost 100% contrast, could be detected in relaxed conditions, more precisely in sizable numerical apertures (NA = 0.4 in air) in spite of the highly multimode nature of the system ($m_{\max} > \sim 40$).

2.2. *Transmission features of finite waveguide*

To guide us in the design of a microresonator, we examine the properties of a waveguide. To this end, we perform 2D finite-difference time-domain FDTD simulations [26] of the structure shown in Fig. 2, deprived of any facets (replaced by "PML", the well-known perfectly matched layer).

With reference to Fig. 3(a), we use as a source, a tilted plane Gaussian "exciter", much as in [16], with frequency centered at the Littrow condition for 45° incidence, and we focus on the most favourable TM polarization (magnetic excitation **H** in the figure plane, electric field **E** normal to the figure and scalar). We found that TE polarization does not offer strong diffraction efficiency for the triangular grating until the aspect ratio is almost prohibitively high ($h/\Lambda > 3$ or so), un fortunately. Given an index $n = 3$ in this first attempt, the central ray of our simulation has a longitudinal wavevector component $(2\pi/\lambda) \times n \sin(45^\circ)$ (an effective index $3/\sqrt{2} = 2.12$) that should coincide with half the grating wavevector π/Λ, hence

$$\lambda = \Lambda\sqrt{2}n \tag{3}$$

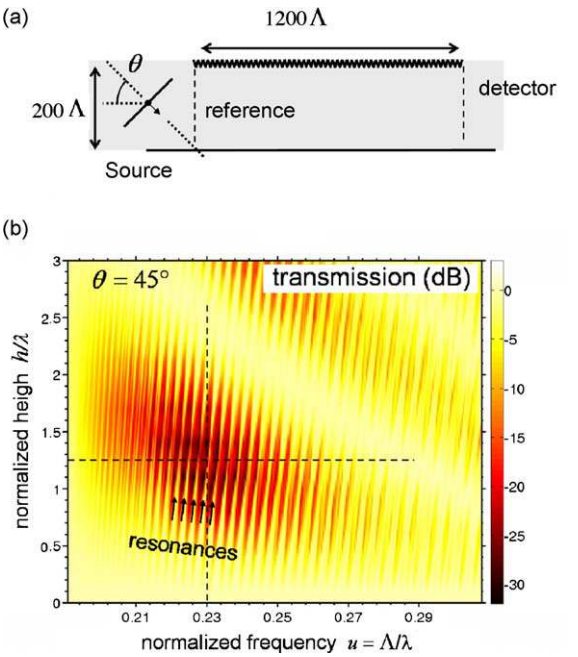

Fig. 3. (a) Constant-height corrugated waveguide section, 120Λ long and 20Λ wide, illuminated by a 45°-tilted source, detection taking place at the end; (b) color map of the resulting transmission intensity as a function of frequency and corrugation height (i.e. groove depth). (For interpretation of the references to color in this figure legend, the reader is referred to the web version of the article.)

meaning also $\lambda = \Lambda \times 2n_{\text{eff}}$, but this latter form is too general. We use normalized frequencies defined by $u = \Lambda/\lambda$, and our central pulse frequency is centered around $u = \sqrt{2}/2n = 0.236$. The length and thicknesses are chosen as 120Λ and 20Λ, to mitigate accuracy and significance for an infinite system.

We obtain the transmission map of Fig. 3(b) by scanning the corrugation height (the groove depth, in other words), recording for each height the transmitted spectra by a detector inside the solid and taking as a reference the detector at the corrugated waveguide entrance. The map clearly reveals the "sweet spot" of the grating behaviour for this selected case of 45° excitation. In this spot, transmission is strongly modulated and its resonance appears as the tenuous light areas (further denoted as "scars") over the locally dark background, that corresponds to light being repelled when it does not hit one of the flat bands. The best grating height appears at $h/\Lambda = 1.25$ We can note here that the traditional rule of echelette gratings, that would here translate in 45° grooves with $h/\Lambda = 0.50$ for 45° Littrow blaze behaviour, is by far no more obeyed for small periods, on account of the massive electromagnetic role of the dielectric corner.

The best frequency is then $u = \Lambda/\lambda = 0.230$. For our thickness, the free-spectral range (FSR) of the resonances is $\Delta u \approx 0.0033$.

(See the Appendix in [16]. In brief, the relevant "Littrowian" round-trip optical path for 45° rays in a thickness e at 45° is $4ne\sqrt{2}$, hence an order $m = 4ne\sqrt{2}/\lambda$ and a free-spectral range $\Delta u/u \cong 1/m = \lambda/4ne\sqrt{2}$. Here $e = 20\Lambda$, and thus $m = 80n\sqrt{2}\Lambda/\lambda = 80$, which underestimates the FSR at $u = 0.23$, notably because of the grating depth not being taken into account upon using the optical path unetched thickness e instead of a diminished effective thickness.)

Admittedly, we do not generate a single guided mode with our Gaussian excitation, but the deep modulation of the transmission shows that we have properly hit the tenuous stripes of photonic bands spaced by the broad stripe of minigaps of the system. We do not see substantial differences unless we widely change the source lateral extent. This is a first good sign that the devices investigated here lend themselves to a good coupling with standard focused beams, unlike more commonly addressed single-piece microresonators.

To investigate the angular tolerance of the fine transmission features evidences above, we scan the tilt of the source over 35° of *internal* angle, which is about what can be obtained by a 180° scan of the incidence from the air at the facets of the prism studied below. We set the height at $h/\Lambda = 1.25$, the best value found above.

The resulting transmission map vs. frequency and angle (Fig. 4(a)) shows that there are more margins on the large angle side. The transmission modulation is up to about 30 dB. The finest resonances are magnified in Fig. 4(b), around the design frequency. Outside this region, they evolve into more square modulations bands at high (or low) frequencies, much as the trend observed in [22]. This shows that we have the flattest bands and narrowest peaks at the design frequency, and that we recover bands with "faster" light and more frequency span at higher frequencies. To help the reader to grasp a complete view, we gather in Fig. 4(c) the two above color maps into a perspective of a cut colored volume (transmission vs. angle, frequency and depth). The design region is thus well defined in terms of frequency, corrugation depth and angle. The maximum depth of

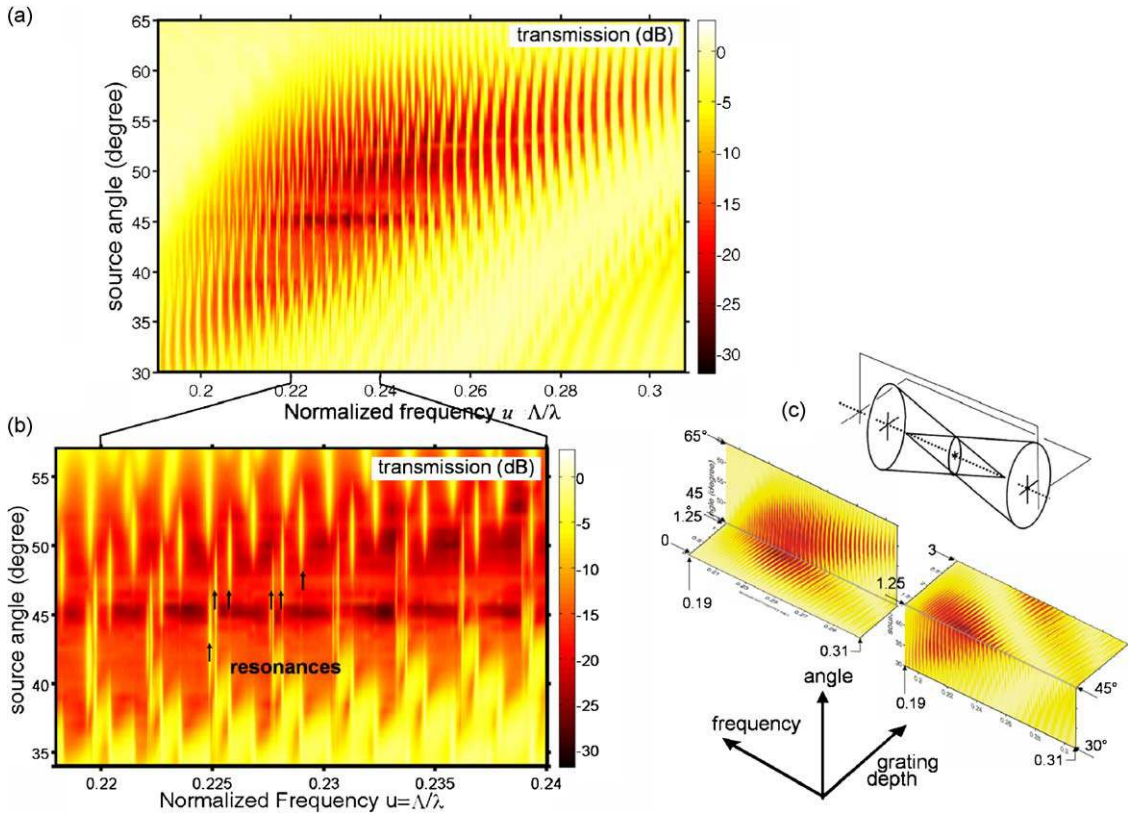

Fig. 4. Transmission maps of the same system as previous figure: (a) transmission map vs. frequency and source angle; (b) magnified region showing split resonances due to the finite waveguide length; (c) "cut-box" of the volume map obtained by collating the angular and height-dependent data, highlighting the overall shape of the strong interaction region, consisting of two fuzzy cones.

modulation of the transmission indicates that the overall topology of the region of maximal feedback lies at the intersection of two fuzzy cones, sketched in Fig. 4(c). A last aspect that we can view on these maps is the role of the finite simulation extent. Instead of having a continuous resonant ''scar'' vs. angle at resonant frequencies, the scar splits in several somewhat symmetric features (Fig. 4(b)). We attribute this to the unavoidable quantization of longitudinal wavevector arising in the finite model system.

This remark opportunely provides us a transition: we should next consider proposing an actual microresonator with the smallest possible discrete modes and design a feasible input/ouput geometry. Our next step is therefore to shape the ''optical access'' to a finite fraction of such an opened resonator, in order to get a structure exhibiting fully discrete modes. This will still be done here in two dimensions, letting the third dimension frozen. This freezing may arise through waveguiding in the third dimension (as in microdisks), or, conversely, because the beams used have negligible divergence along this third direction, meaning that all optical paths of interest have to be smaller that the Rayleigh length along the longitudinal light path associated with the beam waist in this third dimension.

Also, we will move to a more realistic material, silicon, with a higher index $n_{\mathrm{Si}} = 3.45$. One obvious consequence is to lower the normalized frequency region $u = \Lambda/\lambda = 1/(\sqrt{2}n_{\mathrm{Si}})$ from $u \sim 0.23$ to $\sim$0.205 (normalized Bragg frequencies scale like $1/n$). The optimal depth increases a little above $h/\Lambda = 1.30$. We think that it was nevertheless useful to assess the broad corrugated waveguide properties in the case $n = 3$, because key phenomena were more clear in this case. But all phenomena, notably the extent of the ''sweet spot'', are essentially unchanged for this larger index.

3. Prism-type Littrow resonator

3.1. Geometrical design

Based on the geometrical rays, we show in Fig. 5 the layout of a device consisting of a trapezoidal prism (here at 45°) with one face formed intro a grating with a triangular profile (this choice of profile could be changed, but the triangular shape provides a modal simplicity, as outlined recently in the different context of polarization effects [27]). The dimensioning is based here on the number of successive reflections allowed.

If one want a resonator behaviour and the ''semi-planar'' geometry of Fig. 5, at least two separate coherent reflections on the grating should take place. The 45°

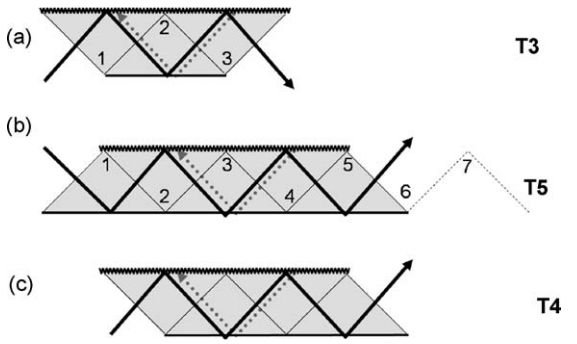

Fig. 5. Trapezoid prism design rule: (a) smallest case, tiled with three triangles (T3); (b) semi-planar case, five triangles (T5); in the case of (T4), light exits on the opposite side and is unchanged in direction.

input/output facets define entrance and exit pupils. They can be antireflection coated at a first stage, because otherwise, the interplay of facet and resonator reflections adds undesirable complexity. Note that the 45° choice makes the ''best use'' of light, i.e. it minimizes the resonator volume. More obtuse angles lengthen the device, whereas more acute ones reduce the input pupil. Still, the 45° choice puts a limit on effective total internal reflection, and therefore on the range of indices that may work. The present proposal is therefore targeting high indices (typically semiconductor ones), but it would be interesting to extend it to the index of organic materials (1.6 or so), for which 45° internal TIR still works with air as the surrounding medium.

This being said, it appears clearly that the design amounts to tile in a ribbon a proper number T of 45°/45°/90° triangles. The smallest design is $T = 3$ (Fig. 5(a)), but requires that 45° pupils direct the impinging light straight on the grating. We envision that the grating will preferably be elaborated on top of the trapezoidal prism, and that its basis could rest on a flat low index material such as silica. Therefore, top access for both input and output beams (what we term ''semi-planar'') involves that $T = 5$ (Fig. 5(b)) is the minimal design. Designs with $N + 2C$ triangles can then be seen as C coupled resonators of the $T = 3$ type, and the analogy can be pursued with the ''CROW'' [28] or other coupled resonators. The variant of Fig. 5(c), which conserves the input/output beam direction, could be adapted to resonators made from very thin active crystals, cut and polished from the bulk, rather than crystals grown on a substrate.

3.2. Optical properties

To study the transmission of such trapezoidal prisms with gratings, we again exploited FDTD simulations. A

typical design is shown in Fig. 6(a). The prism bottom rests on an $n = 1.5$ basis and is clad by air on top. This is a typical configuration if the prism is carved in a thick silicon onto a silica layer.

Admittedly, the obtainment of 45° flat facet is a technological difficulty yet, and for this reason we later address a vertical grating-coupled design in the next paragraph (the (1 1 1) faces of a silicon (1 0 0) wafer could be exploited to alleviate these technological difficulties as well, but this seems a particular case). It is nevertheless useful to check that the present finite implementation with well-defined entrance and exit pupils does work as an original microresonator. Its insertion loss can be optimally low thanks to the antireflection coating. We recall also that AR coating are much less delicate than HR ones, thus this minor deviation from the ''single material'' philosophy underlying this proposal is still benign.

Fig. 6(b) presents, to fix the idea, the resonant field for an $m = 30$th order simulation ($m = 4ne\sqrt{2}/\lambda$, i.e. successive orders at BZ edge are separated by $\Delta\lambda \sim 50$ nm at 1550 nm). The field (here the scalar E_y component of the electric field) is seen to explore the grating up to the tip, except in the middle of the prism where the tails of all interacting modes (two forward and two backward modes) apparently tend to produce an overall field that locally skims under the teeth instead of penetrating in them. Obviously, at this stage, the interplay of finite size with the very essential ingredients (period, thickness) may affect details of the result.

With this idea in mind, let us examine transmission spectra and their peaks (Fig. 6(c) and (d)). To reach fairly high-Q values, and sample the grating reflection by more resonator peaks, we choose a slightly thicker design at $m = 50$, and $h = 1.35a$.

Overall, a fairly good coupling is observed: for the mode at the center of the design (1576.3 nm) Q is about 4000. The transmission is -5 dB, which might not seem very high. Other modes have lower Q (typically down to 2000), but reach almost -1 dB (around 1513 nm). Hence the sharp resonances identified in Figs. 3 and 4 are observed in this basic design.

A more specific effect of the finite grating size can be seen when scanning the groove depth h (Fig. 7(a): graph with inset in the case $m = 39$; Fig. 7(b): map in the case $m = 50$). The resonance surprisingly plummets around the best design, the one associated to the highest apparent transmission contrasts in the less detailed waveguide studies above. High-Q and reasonably good transmission are retrieved only for h values reasonably off the central value, presently $h \sim 1.33a$ (this central value slightly depends on m, having $\Delta h \sim 0.05a$ typical

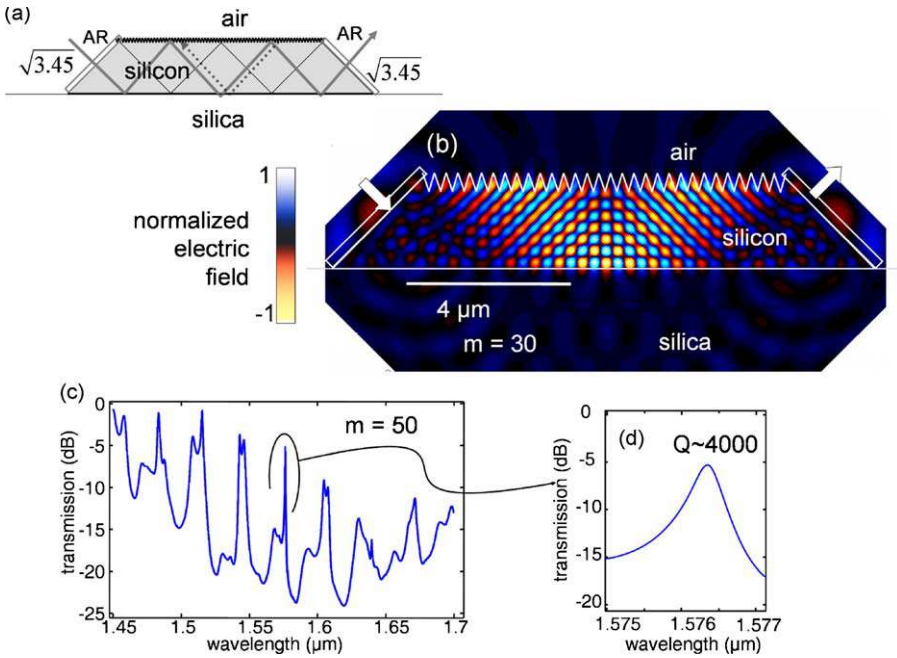

Fig. 6. Trapezoid prism made of silicon (index 3.45) with AR coatings at the input facet; (b) color map of the most resonant field, the one surviving the excitation for the longest time, in a $m = 30$ trapezoidal prism; (c) transmission spectrum of a $m = 50$ system around 1550 nm, for $h = 1.35a$; (d) magnified transmission of the narrowest peak, offering $Q = 4000$ at nearly -5 dB. (For interpretation of the references to color in this figure legend, the reader is referred to the web version of the article.)

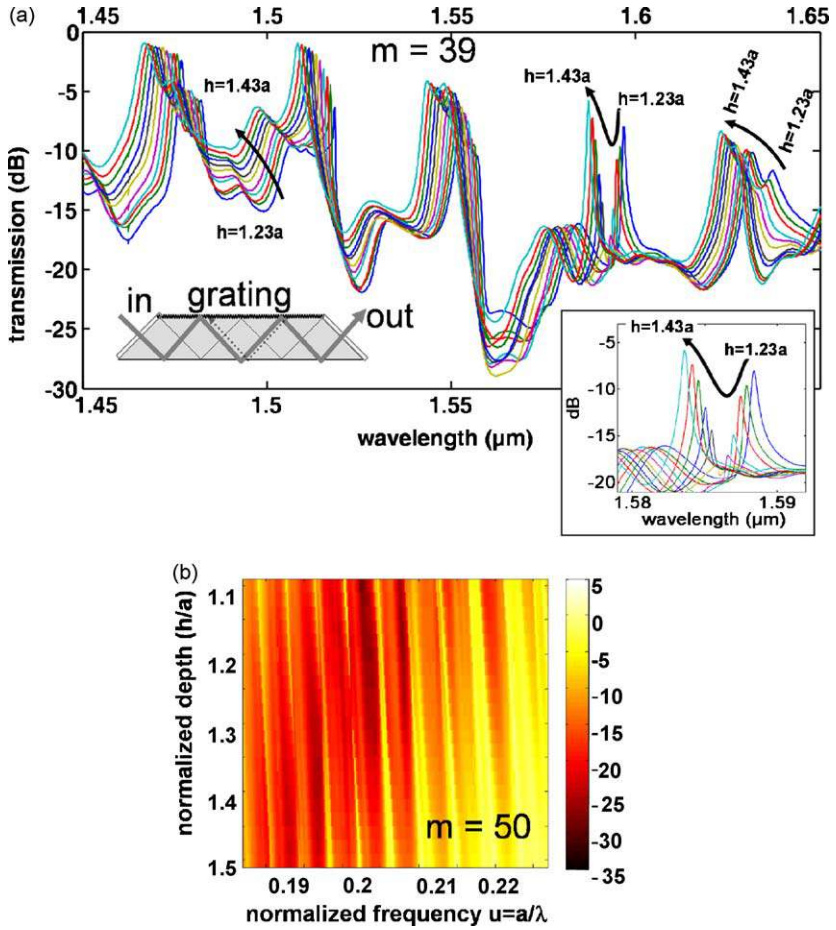

Fig. 7. Grating height scan of spectra of the $m = 39$ system around the best values $h = 1.23a$ to $1.43a$, showing that the resonance goes through a minimum (inset); (b) transmission map (vs. frequency and depth h/a) for the reference case $m = 50$, showing the same vanishing "scar" in the most efficient diffraction region.

fluctuations for the sizes $m = 30...50$ we investigated). We cannot attribute this to a multipole cancellation effect (see [29]), because we unambiguously assessed an absence of singular Q increase when investigating small enough simulations ($m = 39$ in Fig. 7(a)) that offer high enough frequency resolution to be conclusive.

We anticipate that various design refinements should help taming this unforeseen phenomenon and would give very good performances to our resonators: for example, one may impose a grating phase shift of a half period in the device center, or a small symmetric chirp of the grating period, to mimic cavities with curved mirrors, etc. We have tried explicitly one of the simplest arrangement, which is to change the relative symmetries of the 50 teeth (there are m teeth) of the grating with respect to the prism by a half-period ($\Lambda/2$) relative translation, but without clear effect. We find that a minority fraction of the modes also exhibits this resonance cancellation effect, but the one at the center of the nominal design set is the more clear case. But a majority of the lower Q modes just gently shifts in frequency with increasing grating depth, following a very smooth variation of Q and of peak transmission, free from cancellation.

An important aspect of our design is its ability to couple the resonant mode with beams of reasonable practical extent with a large tolerance, an ability rather absent (if ever addressed) in microcavity designs based on arrangements of successive internal reflections more than on diffraction. To show this ability for our design, we vary the input source angle by $\pm 7^\circ$ in air and observe how transmission at the output is affected. This corresponds to assessing rays across a NA ~ 0.1 aperture. The properly weighted average of such data, in a $[-\theta, +\theta]$ window would, to first order, inform us on the coupling vs. beam aperture. We will get here an upper bound of the degradation by considering the largest angle.

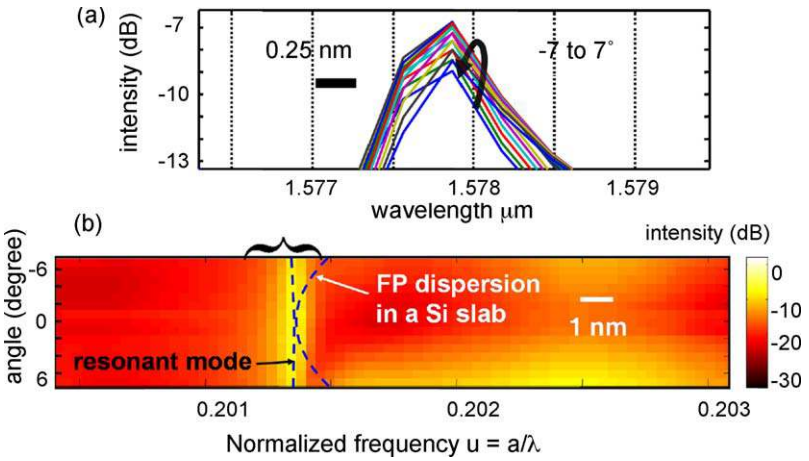

Fig. 8. Angular sensitivity of the trapezoidal prism; (a) collated spectral transmission data for $\pm 7^\circ$, showing fair tolerance; (b) same results plotted as a transmission map; the brace covers the above graph, and the parabolic dashed line reproduces a typical Fabry-Perot dispersive behaviour.

The results in Fig. 8(a) and (b) relate to the $m = 50$ case and $h = 1.20a$. Selecting a higher m is more significant to show that the resonance is very stable in frequency and acceptably constant in coupling level all over the range investigated: a limited 2 dB span is seen. Depending on the application, this may be deemed as fairly constant, or not very satisfactory, but we believe it is a good starting point for the class of systems we are interested in. It is difficult to define a broadly acceptable figure of merit here, although the general perception is, we believe, accepted among practitioners: at the extreme, a sphere's Mie resonance accepts any excitation angles in 3D, and a microdisk similarly in 2D, but the they do not couple easily all incoming light. As for the wavelength stability, the centroid of the peak moves by quite less than 0.25 nm over the range in question. This compares favourably with the case of a similar silicon-based planar microcavity: this planar cavity would experience a wavelength scaling at best like $\cos(\theta/n)$ and hence a relative shift $\delta\lambda/\lambda = 1/2(\theta/n)^2$, of 6.2×10^{-4} in the present case, that is about 1 nm. The corresponding dispersion is rendered in the map of Fig. 8(b), made on a broader frequency span.

It is thus clear that our microcavity design, while physically open, exhibits genuinely frozen eigenmodes, and clamps the resonant wavelength with a 5–10 times better accuracy vs. coupling angle, at least, than an unlimited equivalent Fabry-Perot. It is a genuine resonator, and not a particular implementation of a planar cavity: the finite size is properly managed as the mode covers the whole grating with a proper profile, much as the mode profile covers the cross-section in high-Q micropillars.

Again, we do not provide more data because still design work has to be done to fine-tune the device. A more exact coupling-tolerance simulation set can also be devised, with off-centered Gaussian beams, or Gaussian beams of variable (matched or mismatched) waist diameters. The absence of such data for reported microcavities prompts us to postpone this in further publications. A noticeable related case of some interest for comparison, however, might be found in tapers, for which coupling tolerance is very well documented, including in experiments (see also [15]). We follow here a different philosophy, suppressing the translationally invariant stage of the ridge/rib ''access'' waveguide connecting input/output tapers to the resonator, in order to also retain genuine miniaturization prospects meant for extensive multi-device operation a chip.

4. Top access double-pitch double-grating resonator

In order to get resonators whose excitation can be performed near-vertically from the top of their supporting substrate, we attempt to perform in- and out-coupling through two symmetric gratings (Fig. 9(a)). The input grating, for instance, receives a collimated vertical beam and should ideally diffract it at 45° in its first order at the design wavelength, so that the beam then follows the same fate as in the previous case with the 45° facet. It is elementary to conclude that the pitch of this grating is $\Lambda_2 = 2\Lambda$, twice the pitch of the central ''feedback'' grating.

We opt for a simple saw-tooth grating with vertical sidewalls to get near to the blazed situation, and of course still to silicon ($n_{\mathrm{Si}} = 3.45$) as the device material. It is notoriously difficult, at such high angles and high index, to make transmission gratings blazed in their first

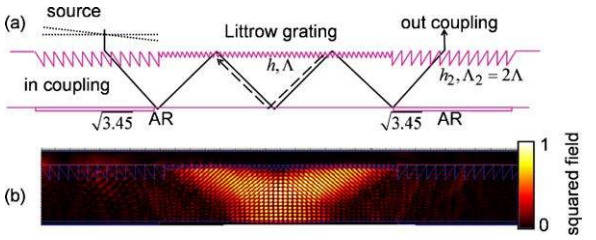

Fig. 9. (a) Sketch of the system with double period saw-tooth coupling grating comprising only 13 teeth here. Note the AR bottom coating provisionally added to kill unwanted vertical reflections; (b) snapshot of the resonant ringing mode squared field, analogous to the trapezoidal prism.

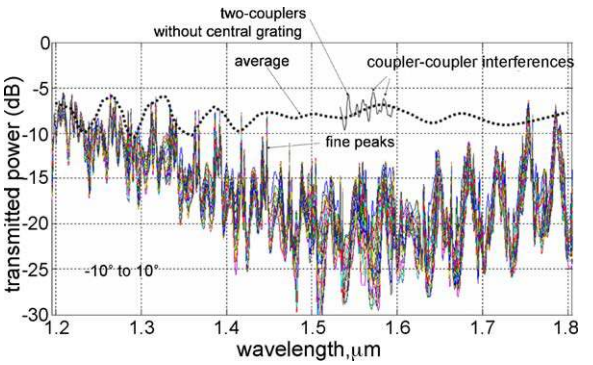

Fig. 10. Transmission spectra vs. source angle for the two-couplers + Littrow grating resonator. The dashed and the thin solid black lines are for a virtually grating-less case, with fine features conserved (thin line) or averaged (dashed line); the other bunch of spectra (color online) are for a case with a grating as before ($h = 1.35a$), and scanning the source tilt over $\pm 10^\circ$ by 1° steps. Peaks at the short wavelength side are seen to best survive, with -8 dB overall transmission. (For interpretation of the references to color in this figure legend, the reader is referred to the web version of the article.)

order. Hence we only optimized the depth of the saw-tooth profile to produce maximum diffraction efficiency and good $+1/-1$ directionality. The output grating is then, obviously, merely symmetrical.

We reached an efficiency of 50–60% per coupler for a teeth depth $h_2 = 1.57\Lambda_2$, nearly a 60° slope of these double-width teeth. Then, we have to mitigate the normal incidence Fabry-Perot behaviour of light in the zero order (propagating vertically up or down). The interferences of this process tend to affect both the input and output efficiency, since waves reflected at the silicon layer bottom cause constructive or destructive effective diffraction efficiency at 45° in the desired oblique order. We cancel this effect simply by an AR coating on the bottom, at this stage: we stick a quarter-wave thickness piece of index $\sqrt{n_{si}} \approx 1.86$ under the coupling grating, and nothing right in the middle, to avoid interaction with the central series of three total internal reflection at 45° (these waves' effective index is above 2.4, but we want to keep a large margin). This is shown in Fig. 9(a).

To probe this design numerically, by FDTD, we position a Gaussian source on top of the input grating, shining light at a central angle between $+10^\circ$ and -10° off the vertical axis (the device normal).

Fig. 9(b) shows the final state in one of the resonant cases described further below, where the localization effect exploited in the prism case is reproduced in essence.

In Fig. 10, we show the various spectra on a broad scale. Firstly, for an almost grating free case ($h/a = 0.01$), the thin solid line whose only a sample is shown, is measured. This is essentially a measure of the couplers overall efficiency, the Littrow grating having negligible effect in this case. We see an average value around -7 dB, in agreement with the $\sim$50% coupling efficiency, with likely an extra 1 dB loss arising from the loss of collimation upon the zigzag path. The fine fringes of this "reference" case correspond to the occurrence of the Littrow -2 reflection order on the coupling grating, allowing light to bounce between the couplers. The fringe visibility suggests a typical 15–20% reflection, rather less than a bare Si/air interface, but still not perfect.

The thick dotted line is a visual average of such fringes, plotted on the whole range. It accounts for the coupling efficiency more meaningfully than the oscillating curve, as the transmitted complex amplitude between the couplers will be drastically affected in the presence of the grating, and the fringes should not show up the same way at all.

The bunch of thin solid curves is the transmission for the 21 angles investigated (-10° to 10° per 1° step). The main trend of a broad transmission "trough" is similar to that of Fig. 4(a), with levels on the sides of the trough recovering about unit transmission with respect to the coupler. The trough is nevertheless scarred by fine resonances that are due to the central grating as expected. Here, the peaks at the wavelengths previously identified around 1580 nm are somewhat merged in the background slower oscillations. Only the peaks in the window 1400–1500 nm do form neater resonances. This surprise might stem from unwanted dispersion and distortion of the in-coupled wavefront by the grating coupler, a possible effect that we still have to work out. It is certain that the price of vertical coupling is a larger design effort.

To detail a little more these resonances, we plot a zoom of their good region in Fig. 11(a). It reveals Q

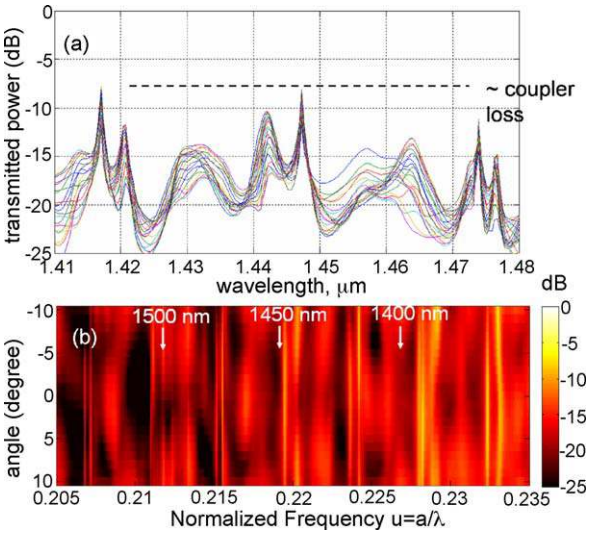

Fig. 11. Same as the figure above, but magnified to see the detail. (a) Magnified transmission spectra: peaks reach the average coupler loss, meaning that the core of the resonator has very good properties. (b) Transmission map as a function of normalized frequency and angle, where the resonance intensity and the minute dispersion vs. angle can be assessed.

factors of the same order as seen previously for this $m = 50$ design (30 nm FSR), that is above 2000, and hence equivalent finesses $F = Q/m$ above 40.

Fig. 11(b) shows that again, there is no angular sensitivity on the resonance frequencies, and still a large window for each of them, with typical 3 dB variations across almost the 20° full aperture zenithal angle.

Thus, not only can a collimated Gaussian beam (beam size 7–8 μm) be used, but also the alignment tolerance may be relaxed by 5° or even 10° while preserving decently functional resonances.

5. Conclusion

We have proposed an approach starting from bandstructure considerations and going to practical microresonator implementation based on Littrow grating and total internal reflection in a slab having the grating on one side. We slightly tuned some parameters during the investigation (such as the index, from $n = 3$ to 3.45, or the groove depth, around $h = 1.3a$) confirming that the design rules on thickness and on grating height (grooved depth) are quite clear and tangible. The depth of the groove has a clear optimum for a given index, at the nominal Littrow condition. To exploit the flat bands stemming from the coupling of guided modes around the efficient Littrow diffraction, the shape of a trapezoidal prism with 45° facets can be first exploited. The basic design uses five underlying triangles and was called T5 for this reason, but other longer designs can be devised, and the device shall then behave somewhat as a "CROW" (coupled resonator optical waveguide [28]). We have found Q values of around 4000 for this first design attempt, and an order $m = 50$, hence finesses slightly under $F = 100$. The main assessment of large angular tolerance, was shown for a 7° half-angle, and the resonance stability upon angular variations was found to be vanishingly small, showing that this resonator undoubtedly goes beyond a mere "grating-folded" planar Fabry-Perot. The device can, in our opinion, be classified as a microcavity, having (at $\lambda = 1.55$ μm design) its input facet size substantially smaller than the diameter of a typical single-mode fiber. The counterpart of the wavelength "stability" is the existence of various finite size effects (primarily lower Q at smaller sizes but more generally a complex transmission "floor" between resonances). They have been tackled to a limited extent in order to defined future work direction.

Eventually, a more complex device incorporating two extra gratings for input- and output-coupling was devised and modeled. The couplers somewhat limit the absolute performance and may blur the neatest design region, but still, the angle-tolerant and high-Q resonant behaviour were identified, provisionally fulfilling the target of a resonator made almost of a single piece of material (no multilayer, no air gap) but showing good optical characteristics by making good use of Littrow reflection rather than ubiquitous but angle-sensitive Fresnel reflection at large incidence.

As a final note, we mention that the approach may be extended to other waves that have similar velocity behaviour among different media, e.g. acoustic waves.

Acknowledgments

This work was carried out in the framework of the CNano IdF "POLYKAPPA" project. The author is indebted to O. Khayam, C. Cambournac and M. Barut (during his internship) for their help and suggestions.

References

[1] K.J. Vahala, Optical microcavities, Nature 424 (2003) 839–847.
[2] T. Ben-Messaoud, J. Zyss, Unidirectional laser emission from polymer-based spiral microdisks, Appl. Phys. Lett. 86 (2005) 241110.
[3] R. Dubertrand, E. Bogomolny, N. Djellali, M. Lebental, C. Schmit, Circular dielectric cavity and its deformations, Phys. Rev. A 77 (2008), 013804 (1-16).

[4] B. Gayral, J.M. Gérard, A. Lemaître, C. Dupuis, L. Manin, J.L. Pelouard, High-Q wet-etched GaAs micropillars containing InAs quantum boxes, Appl. Phys. Lett. 75 (2001) 1908–1910.

[5] M.R. Watts, S.G. Johnson, H.A. Haus, J. Joannopoulos, Electromagnetic cavity with arbitrary Q and small modal volume without a complete photonic bandgap, Opt. Lett. 27 (2002) 1785–1787.

[6] A. Karalis, S.G. Johnson, J.D. Joannopoulos, Discrete-mode cancellation mechanism for high-Q integrated optical cavities with small modal volume, Opt. Lett. 29 (2004) 2309–2311.

[7] S. Reitzenstein, C. Hofmann, A. Gorbunov, M. Strauß, S.H. Kwon, C. Schneider, A. Löffler, S. Höfling, M. Kamp, A. Forchel, AlAs/GaAs micropillar cavities with quality factors exceeding 150.000, Appl. Phys. Lett. 90 (2007) 251109.

[8] M. Born, E. Wolf, Principles of Optics, Cambridge University Press, Cambridge, 1999.

[9] S.V. Boriskina, T.M. Benson, P. Sewell, A.I. Nosich, Optical modes in 2-D imperfect square and triangular microcavities, IEEE J. Quant. Electron. 41 (2005) 857–862.

[10] S.V. Boriskina, T.M. Benson, P. Sewell, A.I. Nosich, Q factor and emission pattern control of the WG modes in notched microdisk resonators, IEEE J. Sel. Top. Quant. Electron. 12 (2006) 52–58.

[11] S.V. Boriskina, T.M. Benson, P. Sewell, A.I. Nosich, Directional emission, increased free spectral range, and mode Q-factors in 2-D wavelength-scale optical microcavity structures, IEEE J. Sel. Top. Quant. Electron. 12 (2006) 1175–1182.

[12] N.B. Rex, H.E. Tureci, H.G.L. Schwefel, R.K. Chang, A.D. Stone, Fresnel filtering in lasing emission from scarred modes of wave-chaotic optical resonators, Phys. Rev. Lett. 88 (2002) 094102.

[13] W.H. Guo, Y.Z. Huang, Q.Y. Lu, L.J. Yu, Whispering-gallery-like modes in square resonators, IEEE J. Quant. Electron. 39 (2003) 1106–1110.

[14] Y.Z. Huang, W.H. Guo, Q.M. Wang, Analysis and numerical simulation of eigenmode characteristics for semiconductor lasers with an equilateral triangle micro-resonator, IEEE J. Quant. Electron. 37 (2001) 100–107.

[15] F. Van Laere, T. Claes, J. Schrauwen, S. Scheerlinck, W. Bogaerts, D. Taillaert, L. O'Faolain, D. Van Thourhout, R. Baets, Compact focusing grating couplers for silicon-on-insulator integrated circuits, IEEE Photon. Technol. Lett. 19 (2007) 1919–1921.

[16] H. Kurt, H. Benisty, T. Melo, O. Khayam, C. Cambournac, Slow-light regime and critical coupling in highly multimode corrugated waveguides, J. Opt. Soc. Am. B 25 (2008) C1–C14.

[17] S.H. Kim, S.K. Kim, Y.H. Lee, Vertical beaming of wavelength-scale photonic crystal resonators, Phys. Rev. B 73 (2006) 235117.

[18] B.-S. Song, S. Noda, T. Asano, Y. Akahane, Ultra-high-Q photonic double-heterostructure nanocavity, Nat. Mater. 4 (2005) 207–210.

[19] Y. Akahane, T. Asano, B.-S. Song, S. Noda, High-Q photonic nanocavity in a two-dimensional photonic crystal, Nature 425 (2003) 944–947.

[20] I.-K. Hwang, G.H. Kim, Y.H. Lee, Optimization of coupling between photonic crystal resonator and curved microfiber, IEEE J. Quant. Electron. 42 (2006) 131–136.

[21] O. Khayam, C. Cambournac, H. Benisty, M. Ayre, H. Brenot, G.H. Duan, W. Pernice, In-plane Littrow lasing of broad photonic crystal waveguides, Appl. Phys. Lett. 91 (2007), 041111 (1-3).

[22] O. Khayam, H. Benisty, C. Cambournac, Experimental observation of minigap stripes in periodically corrugated broad photonic wires, Phys. Rev. B 78 (2008), 153107 (4).

[23] L. Martinelli, H. Benisty, O. Khayam, G.H. Duan, H. Heidrich, K. Janiak, Analysis and optimization of compact demultiplexer monitor based on photonic crystal waveguide, IEEE J. Lightwave Technol. 25 (2007) 2385–2394.

[24] S. Olivier, H. Benisty, C.J.M. Smith, M. Rattier, C. Weisbuch, T.F. Krauss, Transmission properties of two-dimensional photonic crystal channel waveguides, Opt. Quant. Electron. 34 (2002) 171–181.

[25] S. Olivier, M. Rattier, H. Benisty, C.J.M. Smith, R.M. De La Rue, T.F. Krauss, U. Oesterle, R. Houdré, C. Weisbuch, Mini stop-bands of a one-dimensional system: the channel waveguide in a two-dimensional photonic crystal, Phys. Rev. B 63 (2001), 113311 (1-6).

[26] See http://www.photond.com/products/crystalwave.htm.

[27] J. Zheng, C. Zhou, J. Feng, B. Wang, Polarizing beam splitter of deep-etched triangular-groove fused-silica gratings, Opt. Lett. 33 (2008) 1554–1556.

[28] A. Yariv, Y. Xu, R.K. Lee, A. Scherer, Coupled-resonator optical waveguide: a proposal and analysis, Opt. Lett. 24 (1999) 711–713.

[29] S.G. Johnson, S. Fan, A. Mekis, J.D. Joannopoulos, Multipole-cancellation mechanism for high-Q cavities in the absence of a complete photonic band gap, Appl. Phys. Lett. 78 (2001) 3388–3390.